Talanta 122 (2014) 285–292

Contents lists available at ScienceDirect

Talanta

journal homepage: www.elsevier.com/locate/talanta

Square wave anodic stripping voltammetric determination of Cd^{2+} and Pb^{2+} at bismuth-film electrode modified with electroreduced graphene oxide-supported thiolated thionine

Zou Li [a], Li Chen [a], Fang He [a], Lijuan Bu [a], Xiaoli Qin [a], Qingji Xie [a,*], Shouzhuo Yao [a], Xinman Tu [b], Xubiao Luo [b], Shenglian Luo [b]

[a] Key Laboratory of Chemical Biology and Traditional Chinese Medicine Research (Ministry of Education), College of Chemistry and Chemical Engineering, Hunan Normal University, Changsha 410081, China
[b] Key Laboratory of Jiangxi Province for Persistent Pollutants Control and Resources Recycling, Nanchang Hangkong University, Nanchang 330063, China

ARTICLE INFO

Article history:
Received 27 October 2013
Received in revised form
26 January 2014
Accepted 28 January 2014
Available online 31 January 2014

Keywords:
Cd^{2+} and Pb^{2+}
Square wave anodic stripping voltammetry
Thiolation
Electroreduced graphene oxide–thionine–2-mercaptoethanesulfonate nanocomposite
Electrochemical quartz crystal microbalance

ABSTRACT

Graphene oxide (GO)–thionine (TH) nanocomposite was prepared by π–π stacking. The nanocomposite was cast-coated on a glassy carbon electrode (GCE) to prepare an electroreduced GO (ERGO)–TH/GCE, then 2-mercaptoethanesulfonate (MES) was covalently tethered to ERGO–TH by potentiostatic anodization to form an ERGO–TH–MES/GCE. The thiolation reaction was monitored by electrochemical quartz crystal microbalance (EQCM). Square wave anodic stripping voltammetry (SWASV) was used to determine Cd^{2+} and Pb^{2+} at the ERGO–TH–MES/GCE further modified with Nafion and Bi. Under the optimal conditions, the linear calibration curves for Cd^{2+} and Pb^{2+} are from 1 to 40 μg L^{-1}, with limits of detection ($S/N=3$) of 0.1 μg L^{-1} for Cd^{2+} and 0.05 μg L^{-1} for Pb^{2+}, respectively. The electrode was used for the simultaneous analysis of Cd^{2+} and Pb^{2+} in water samples with satisfactory recovery.

1. Introduction

As it is well known, lead(II) and cadmium(II) are severe hazardous environmental pollutants with toxic effects on living organisms. Obviously, it is important to explore sensitive, rapid and simple analytical methods for dynamic monitoring of Pb^{2+} and Cd^{2+} [1–4]. Electrochemical techniques, especially anodic stripping voltammetry (ASV), have been well-established for determination of trace heavy metal ions including Pb^{2+} and Cd^{2+}, owing to the advantages of low cost, high sensitivity, and great convenience in operation and proven capability of on-line environmental monitoring. Recently, various bismuth-based electrodes have been extensively studied for ASV instead of mercury-based electrodes [5–8], owing to the low toxicity, the ability to form alloys with many heavy metals, simple preparation, wide potential window, and insensitivity to dissolved oxygen at the bismuth-based electrodes. In addition, various chemically modified electrodes bearing surface functional groups with high affinity to heavy metals and their ions have been widely used for ASV analysis of heavy metals with enhanced analytical performance [9–11].

Graphene is a two-dimensional honeycomb lattice packed by monolayer sp^2-hybridized carbon atoms [12], which has attracted tremendous interest due to the large surface area, attractive thermal and mechanical properties, high electrical conductivity and great potential for chemical modification. On the other hand, thionine (TH) (also known as Lauth's violet) is a widely studied dye for biological staining. TH of conjugated π bonds can easily adsorb on graphene or graphene oxide (GO) through π–π stacking, and this nanocomposite has been widely used for chemo-/biosensing [13–15]. However, the thiolation of TH has not been examined for electroanalysis to date, though the thiolated functional materials and the thiol–ene chemistry have attracted great attentions recently [16–18].

Herein, we study the electrochemical thiolation of electroreduced GO (ERGO)-supported TH by reaction of 2-mercaptoethanesulfonate (MES) with TH at its oxidized state, and a new ERGO–TH–MES nanocomposite is thus prepared. Quartz crystal microbalance (QCM) is used for process monitoring and film characterization. A glassy carbon electrode (GCE) modified with ERGO–TH–MES, Nafion and Bi is applied to sensitively detect Cd^{2+} and Pb^{2+} by square wave anodic stripping voltammetry (SWASV).

* Corresponding author. Tel.: +86 731 88865515.
E-mail address: xieqj@hunnu.edu.cn (Q. Xie).

0039-9140/$ - see front matter © 2014 Elsevier B.V. All rights reserved.
http://dx.doi.org/10.1016/j.talanta.2014.01.062

2. Experimental

2.1. Chemicals and apparatus

All electrochemical experiments were conducted on a CHI660C electrochemical workstation (CH Instrument Co.), and a conventional three-electrode electrolytic cell was used. A glassy carbon disk electrode (3 mm diameter) served as the working electrode, a KCl-saturated calomel electrode (SCE) as the reference electrode and a platinum sheet as the counter electrode. A computer-interfaced HP 4395A impedance analyzer equipped with an HP 43961A impedance test adapter and an HP 16092A impedance test fixture was employed in the QCM and electrochemical QCM (EQCM) experiments [19]. AT-cut 9-MHz gold-coated piezoelectric quartz crystals (PQCs, 12.5 mm diameter, Model JA5, Beijing Chenjing Electronics Co., Ltd., China) were used. The gold electrode of 6.0-mm diameter on one side of the PQC was exposed to the solution and connected to the ground terminal of the HP 16092A test fixture, while the other side of the PQC faced air and connected to the nonground terminal of the HP 16092A. Conductance (G) and susceptance (B) of the PQC resonance were measured synchronously on the HP 4395A during the frequency sweep centering at the PQC resonance frequency. A user program was written in Visual Basic (VB) 5.0 to control the HP 4395A and to acquire admittance data via an HP 82341C high-performance HPIB interface card for Windows 3.1/NT/95. A nonlinear least-squares fitting program based on the Gauss–Newton or Gauss–Newton–Marquardt algorithm was written in VB 5.0 for the simultaneous fits of G and B data during experiments [19]. UV–vis spectra were recorded on a UV2450 spectrophotometer (Shimadzu Co., Kyoto, Japan). Fourier transform infrared (FT-IR) spectra were collected on a Nicolet Nexus 670 FT-IR instrument (Nicolet Instrument Co., USA) in its transmission mode, and the films were carefully scraped off from the electrode surface for FT-IR analysis [18].

GO was purchased from XF NANO, Inc. (Nanjing, China). TH was purchased from Sinopharm Chemicals Co., Ltd. (Shanghai, China). MES was purchased from Aldrich (USA). Thioglycolic acid (TGA) and β-mercaptoethanol (ME) were purchased from Alfa Aesar. Nafion (5 wt%, in a mixture of water and lower aliphatic alcohols) was purchased from Aldrich (USA). The diluted 0.25 wt% Nafion solution was prepared with absolute ethanol. All other chemicals were of analytical grade, and all solutions were prepared using Milli-Q ultrapure water (≥ 18 MΩ cm). National standard samples for water monitoring of Pb^{2+} and Cd^{2+} were commercially obtained from Shenzhen StarCare Technology Co., Ltd., China. Phosphate buffer solution (0.10 M, PBS, 0.039 M NaH_2PO_4 + 0.061 M Na_2HPO_4, pH 7.0) and 0.10 M acetate buffer solution (0.049 M NaAc + 0.051 M HAc, pH 4.5) were used. All experiments were conducted at room temperature (25 ± 2 °C) in air atmosphere.

2.2. Procedures

The GO–TH nanocomposite was prepared as follows. The 0.500 mL of 0.50 mg mL^{-1} GO dispersion was obtained by ultrasonication for 30 min, which was then mixed with 0.500 mL of 1.00 mM TH solution at room temperature for at least 24 h. After centrifugation and rinse with water, the GO–TH nanocomposite was redispersed in 1.00 mL ultrapure water for subsequent experiments.

Prior to experiments, the GCE was in turn polished with 1.0 and 0.05 μm alumina powders, and it was then sequentially sonicated in ultrapure water and anhydrous ethanol. Afterwards, the GCE was subjected to potential cycling (−1.0–1.0 V, 0.1 V s^{-1}) in 0.50 mol L^{-1} aqueous H_2SO_4 until the cyclic voltammograms became reproducible. The Nafion/ERGO–TH–MES/GCE was prepared as follows. 1.0 μL of the GO–TH suspension was dropped on a pretreated GCE and the electrode was kept in air until the solvent evaporated. An ERGO–TH/GCE was prepared by scanning the GO–TH/GCE between −1.3 and 1.1 V at 50 mV s^{-1} in 0.10 M PBS (pH 7.0). Afterwards, the ERGO–TH film interacted with MES at a constant potential (1.1 V) in 0.10 M PBS (pH 7.0) containing 5.00 mM MES to form an ERGO–TH–MES/GCE. Then, 1.0 μL of Nafion ethanol solution (0.25 wt%) was cast on the electrode surface and dried in air. Nafion acted here as a binder to stabilize the modified species on electrodes and as a permselective film to alleviate the interferences of anions [20]. In QCM studies, the ERGO–TH film was also prepared similarly on a QCM Au electrode to study its interaction with MES. Control experiments were conducted similarly in the absence of TH.

SWASV measurements were performed in 0.10 M acetate buffer (pH 4.5) containing 400 μg L^{-1} Bi^{3+}. A preconcentration potential of −1.1 V and a preconcentration time of 300 s were applied to the working electrode under stirring conditions. After an equilibration period of 10 s, the square wave anodic stripping voltammogram was then recorded from −1.1 to 0.1 V, and the solution was not stirred in these two steps. The electrode was cleaned for 30 s at 0.3 V to remove the residual metals and bismuth film under solution-stirred conditions. After recording the background voltammograms in 0.10 M acetate buffer (pH 4.5) containing 400 μg L^{-1} of bismuth, cadmium and lead standard solutions were added into the electrolytic cell as required and the measurements were repeated five times for each experiment. All experiments were performed at room temperature (25 ± 2 °C).

3. Results and discussion

3.1. Electrosynthesis and characterization of the ERGO–TH–MES film

The EQCM using a PQC as its central sensing element is a powerful method to monitor many electrodeposition processes with a mass-detection sensitivity down to (sub)monolayer discrimination [19,21–25]. Generally, the EQCM frequency response (Δf_0) can reflect information both on the electrode-mass change and on the change in viscous loading on the electrode, but the simultaneously recorded EQCM response of the motional resistance (ΔR_1) only reflects information on the change in viscous loading on the electrode. Hence, a pure mass-effect should theoretically not change the R_1 value (i.e. $\Delta R_1 = 0$), namely, a pure mass effect should have a very large $-\Delta f_0/\Delta R_1$ value (theoretically $\rightarrow \infty$). In contrast, a pure density–viscosity effect on the 9-MHz PQC resonance possesses a characteristic value of $-\Delta f_0/\Delta R_1 = 10$ Hz Ω^{-1} [19]. Accordingly, the characteristic $-\Delta f_0/\Delta R_1$ value can be used for data interpretation in EQCM studies. Here, the EQCM technique was used to monitor the electrode reactions of interest. At first, the ERGO and ERGO–TH coated QCM Au electrodes prepared as in the Experimental section were used to tether MES by cyclic voltammetry, as shown in Fig. 1. Note here that TH in the ERGO–TH/QCM Au electrode may mainly exist as poly(TH) (PTH) and/or TH oligomers after its preparation by scanning the electrode cast-coated with GO–TH between −1.3 and 1.1 V at 50 mV s^{-1} in 0.10 M PBS (pH 7.0). When an ERGO–TH/QCM Au electrode was swept in MES-free 0.10 M PBS (pH 7.0, Fig. 1A), the frequency decrease due to oxidation of uncovered Au and the frequency increase due to reduction of Au oxides were observed in the potential range of Au redox chemistry (ca. 10-Hz within each cycle) [23]. After 3-cycle CV, the net frequency change in total was within ca. 3 Hz. When an ERGO/QCM Au electrode was swept in 0.10 M PBS (pH 7.0) containing 5.00 mM MES (Fig. 1B), a large thiol-oxidation peak was observed at 1.0 V, accompanying with a frequency decrease. After 3-cycle CV, and the net frequency change in total reached at ca. −36 Hz.

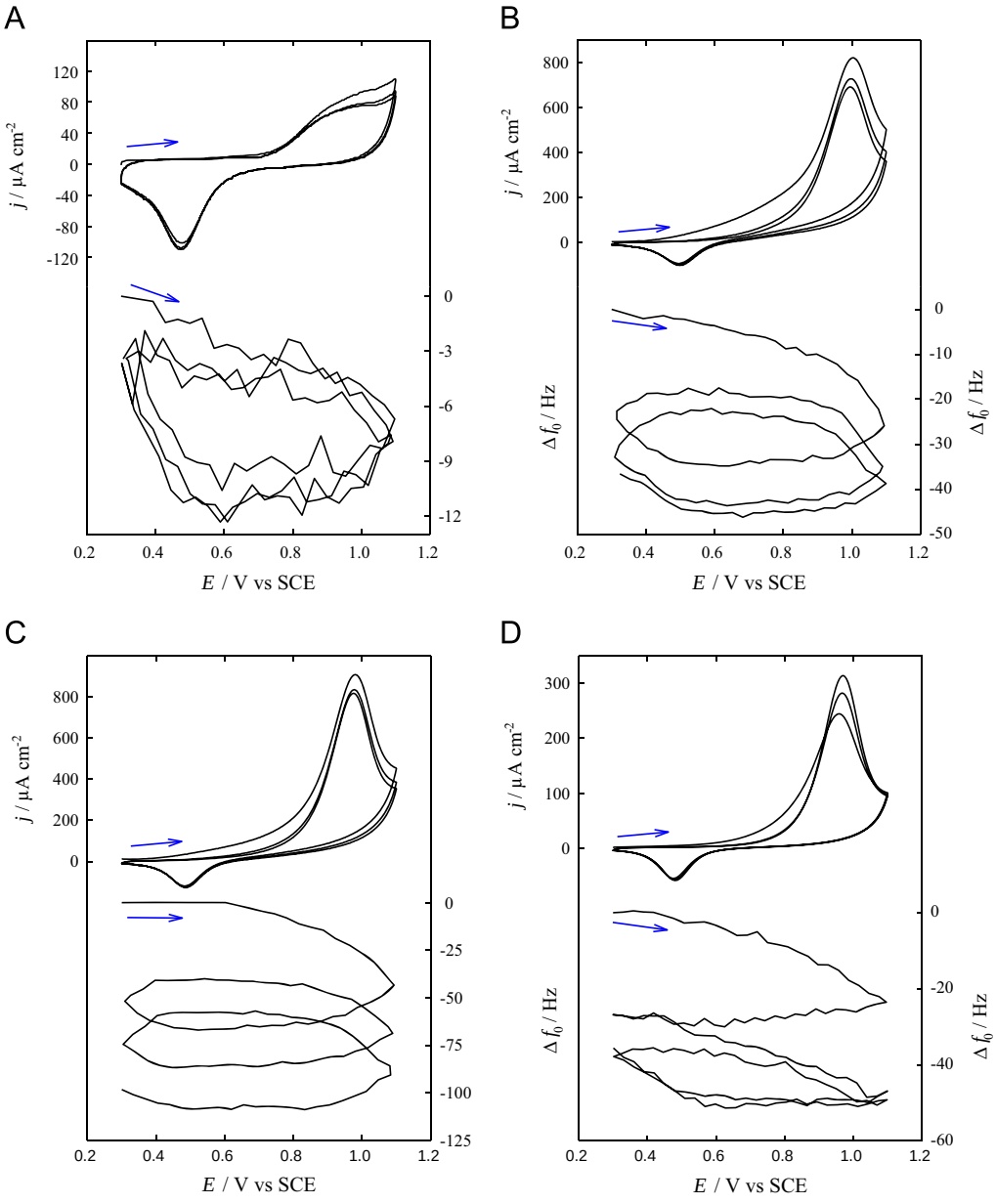

Fig. 1. Cyclic voltammetric EQCM responses of ERGO–TH/QCM Au electrode in 0.10 M pH 7.0 PBS (A), ERGO/QCM Au electrode in 0.10 M pH 7.0 PBS containing 5.00 mM MES (B), ERGO–TH/QCM Au electrode in 0.10 M pH 7.0 PBS containing 5.00 mM MES (C) or PTH/Au electrodes in 0.10 M pH 7.0 PBS containing 5.00 mM MES (D). Scan rate, 50 mV s^{-1}.

In contrast, when an ERGO/QCM Au electrode was swept in MES-free 0.10 M PBS (pH 7.0), no obvious changes were observed (not shown). This phenomenon can be ascribed to the interaction between MES and ERGO, e.g., the reaction of nucleophilic –SH with ERGO of residual quinone groups at anodic potentials. When an ERGO–TH/QCM Au electrode was swept in 0.10 M PBS (pH 7.0) containing 5.00 mM MES (Fig. 1C), a thiol-oxidation peak and the frequency decrease were also observed. After 3-cycle CV, the net frequency change in total reached at ca. −98 Hz, indicating that more MES molecules were tethered to the electrode in the presence of TH. For further verification, we prepared a poly(TH) (PTH)/QCM Au electrode with 60-Hz PTH by CV polymerization of TH, then swept the electrode in 0.10 M PBS (pH 7.0) containing 5.00 mM MES (Fig. 1D). A thiol-oxidation peak was also observed, but the peak current was smaller than that at ERGO–TH/QCM Au electrode, due probably to the absence of large-surface-area ERGO and the presence of a compact electron-insulating PTH film. After 3-cycle CV, the net frequency change in total reached at ca. −38 Hz. However, when a PTH/QCM Au electrode was swept in 0.10 M PBS (pH 7.0), no obvious frequency changes were observed (not shown). These observations indicate that MES can be tethered to TH. Scheme 1 shows the preparation procedures of our Bi/Nafion/ERGO–TH–MES/GCE and the hypothetical structure of TH–MES [26].

We also used the EQCM method to examine the potentiostatic tethering of MES at different electrodes in 0.10 M PBS (pH 7.0) containing 5.00 mM MES. As shown in Fig. 2, when an ERGO–TH/QCM Au electrode was immersed in 0.10 M PBS (pH 7.0) without MES and after the frequency became steady, a static potential of 1.1 V was applied (curve a). A frequency decrease was observed and finally reached −35 Hz after 100 s, corresponding to the formation of Au oxides after this relatively long-time anodic treatment. When the ERGO/QCM Au, ERGO–TH/QCM Au or PTH/QCM Au electrode was subjected to a similar potentiostatic treatment in 0.10 M PBS (pH 7.0) containing 5.00 mM MES (also after the frequency became steady in each experiment), the final

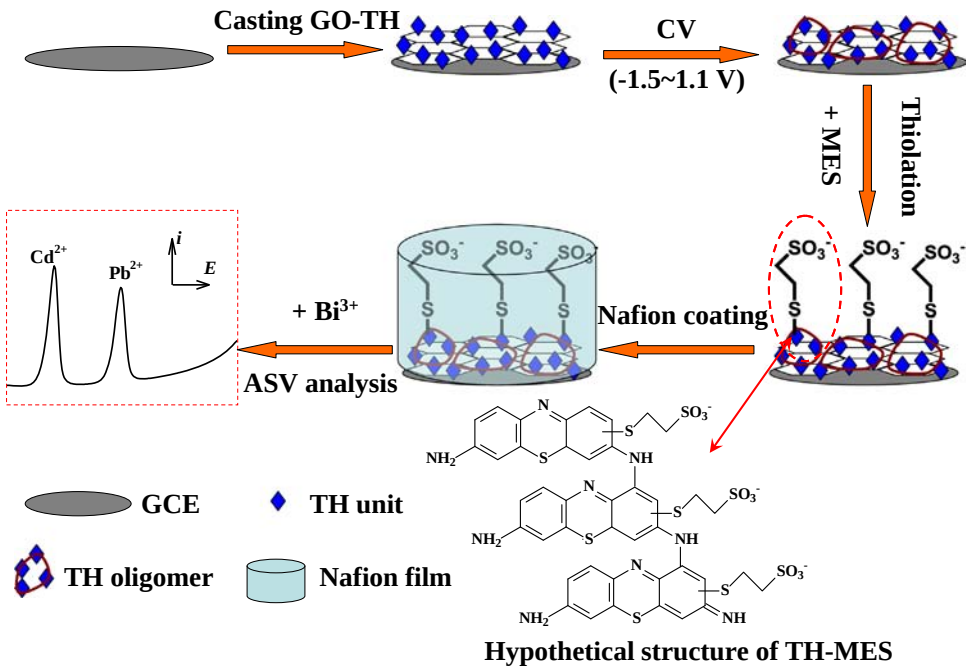

Scheme 1. Schematic illustration of the procedures for preparing the Bi/Nafion/ERGO–TH–MES/GCE for ASV analysis of Cd^{2+} and Pb^{2+} ions (not to scale) and hypothetical structure of TH–MES (here oligomer of TH is assumed) [26].

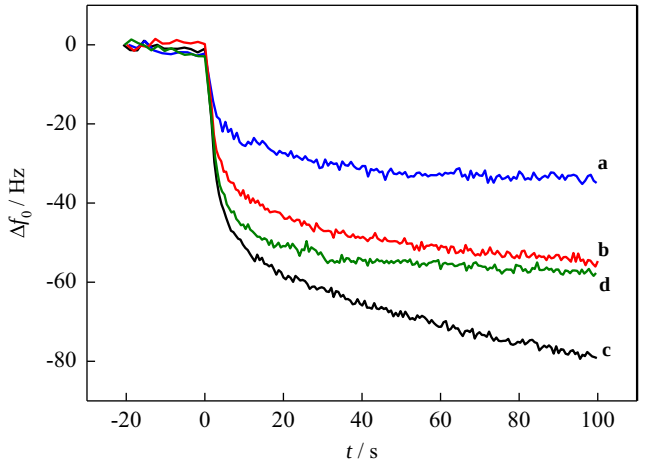

Fig. 2. Time-dependent frequency responses during potentiostatic reaction of ERGO–TH/QCM Au electrode in 0.10 M pH 7.0 PBS (a), ERGO/QCM Au electrode in 0.10 M pH 7.0 PBS containing 5.00 mM MES (b), ERGO–TH/QCM Au electrode in 0.10 M pH 7.0 PBS containing 5.00 mM MES (c) or PTH/QCM Au electrode in 0.10 M pH 7.0 PBS containing 5.00 mM MES (d). Applied potential, 1.1 V. MES was added at 0 s in the cases of curves b-d.

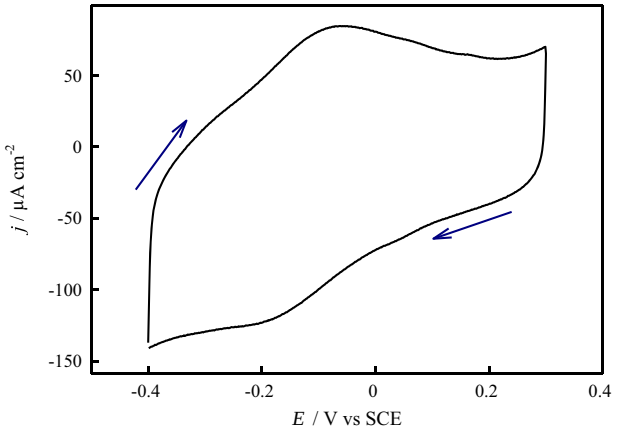

Fig. 3. Cyclic voltammogram of ERGO–TH/QCM Au electrode in 0.10 M PBS (pH 7.0). Scan rate, 50 mV s^{-1}.

net frequency changes in total reached −55, −79 and -58 Hz, respectively. After deduction of formation of Au oxides, it can be roughly estimated that 20, 44 and 23 Hz MES were tethered on ERGO, ERGO–TH and PTH, respectively. The binding molar ratio (r, MES versus TH unit of PTH) for the MES-tethered PTH film at PTH/QCM Au electrode is estimated as follows:

$$r = \frac{\Delta f_{0,\mathrm{MES}} M_{W(\mathrm{TH\ unit})}}{\Delta f_{0,\mathrm{PTH}} M_{W(\mathrm{MES})}} \quad (1)$$

where $M_{W(\mathrm{MES})}$ and $M_{W(\mathrm{TH\ unit})}$ are the molar weight values of MES and the TH unit, respectively, $\Delta f_{0,\mathrm{MES}}$ denotes the frequency shift after the PTH–MES interaction, and $\Delta f_{0,\mathrm{PTH}}$ denotes the frequency shift for the electrodeposition of PTH.

The binding molar ratio (r, MES versus TH unit) values for the PTH–MES interactions were measured from the EQCM data. After 100-s potentiostatic interaction, the r value is calculated to be 0.77. After 3-cycle CV interaction, the r value is calculated to be 1.17.

Redox peaks at −0.18 (E_{pc}) and −0.07 (E_{pa}) V were observed at the ERGO–TH/QCM Au electrode, as shown in Fig. 3, which are due to the electrode reaction of PTH and/or TH oligomers [27]. Similar CV peaks were also observed at modified GCEs, as shown in Fig. S1 with discussion details. Fig. 4 shows the QCM frequency responses to adsorption of Cd^{2+} and Pb^{2+} at bare QCM Au (a), Nafion/QCM Au (b), Nafion/ERGO/QCM Au (c), Nafion/ERGO–TH/QCM Au (d), and Nafion/ERGO–TH–MES/QCM Au (e) electrodes under open-circuit conditions. The Nafion-improved adsorbability could be explained by the fact that the negatively charged Nafion of abundant sulfonate groups can act as a cation-exchanger for electrostatic preconcentration of metal cations [28]. The ERGO-improved adsorbability can be attributed to the presence of the oxygenous groups of ERGO, which can complex with Cd^{2+} and Pb^{2+} [29], and the enlarged electrode active area after

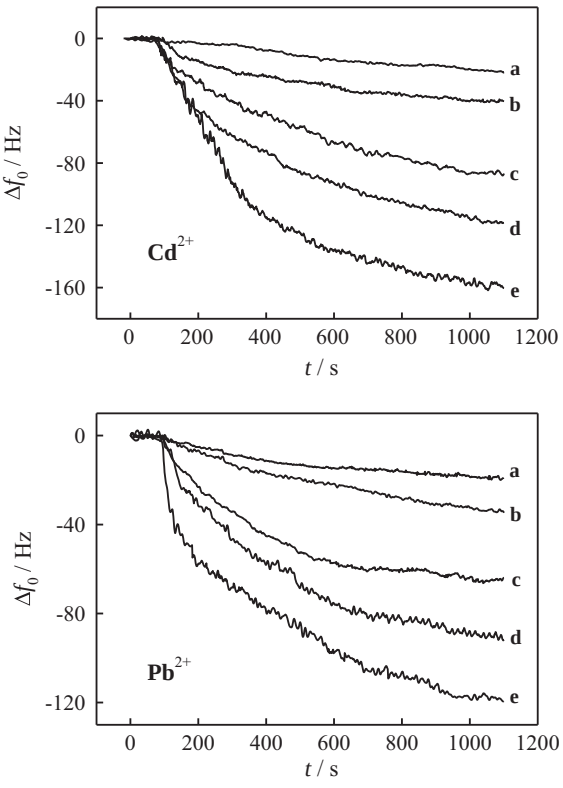

Fig. 4. Time-dependent frequency responses at bare QCM Au (a), Nafion/QCM Au (b), Nafion/ERGO/QCM Au (c), Nafion/ERGO–TH/QCM Au (d) and Nafion/ERGO–TH–MES/QCM Au (e) electrodes to additions of 2.00 mg L^{-1} Cd^{2+} or Pb^{2+} into stirred 0.10 M acetate buffer (pH 4.5).

modification of electron-conducting ERGO nanomaterial. The TH-improved adsorbility could be explained by the fact that S atoms can interact with Cd^{2+} and Pb^{2+} [10]. The MES-improved adsorbability could be explained by the fact that MES contains one S atom which can chelate with Cd^{2+} and Pb^{2+} and one sulfonic group which can attract Cd^{2+} and Pb^{2+} via electrostatic effect [10]. The QCM results here prove that the Nafion/ERGO–TH–MES film shows an enhanced adsorption capacity for Cd^{2+} and Pb^{2+} ions, due to the electrostatic, nanosized and complexation effects as discussed above. It may be argued that the competitive interaction of the film with high-concentration Bi^{3+} ions coexisting in the solution for ASV analysis is obvious, which leads to saturation of the film under the open-circuit condition, and thus the presence of small-concentration Pb^{2+} and Cd^{2+} analytes can yield only a small effect. However, under cathodic preconcentration conditions (−1.1 V, coexisting Pb^{2+}, Cd^{2+} and Bi^{3+}, solution-stirred), the thin-film-bound Bi^{3+}, Pb^{2+} and Cd^{2+} ions can be continuously electroreduced to their atomic states, and thus the active adsorption sites of the film can be continuously refreshed for binding of more Pb^{2+} and Cd^{2+} ions to achieve an enhanced ASV-analysis sensitivity. In other words, under cathodic preconcentration conditions, the active adsorption sites of the film can be continuously refreshed to attract more solution-state Pb^{2+} and Cd^{2+} analytes into the film for their enhanced preconcentration (solution aspect), the codeposited atomic Bi can form alloys with atomic Pb and Cd to decrease the activation energy for cathodic preconcentration of atomic Pb and Cd (surface aspect), and both aspects can enhance the sensitivity of ASV analysis of Pb^{2+} and Cd^{2+} on the target electrode, as experimentally confirmed later.

In addition, UV–vis spectrophotometry was employed to explore the interactions between GO and TH. As shown in Fig. S2, the GO has a characteristic band at 228 nm and a shoulder at 295 nm (curve a), corresponding to π–π* transitions of C=C bonds and *n*–π* transitions of C–O bonds, respectively [28]. The TH solution exhibits two absorption bands (curve b). The absorption bands at 597 and 559 nm correspond to the *n*–π* transitions of C–N bonds in TH, and the main peak at 597 nm is characteristic of monomeric TH, while the 559 nm shoulder can be attributed to the dimer aggregate [30]. The absorption band at 283 nm corresponds to the π–π* transitions of aromatic rings in TH [30]. When TH was mixed with GO (curve c), the slight red shift of those absorption bands are evidences of strong interaction between GO and TH molecules, which is basically consistent with a previous report [30].

Fig. S3 shows the FT-IR spectra of ERGO, ERGO–TH and ERGO–TH–MES film. ERGO (curve a) showed a strong absorption band at 1626 cm^{-1} due to aromatic C=C skeletal vibration [27]. The appearance of peaks at 1400 and 1049 cm^{-1} corresponds to the residual C–O groups [27]. For the ERGO–TH film (curve b), the main peaks near 1569 cm^{-1} can be assigned to the bending vibrations of N–H in PTH structure [27], indicating the presence of TH in the nanocomposite film. After interaction with MES, new peaks at 1202 cm^{-1} (S=O stretching vibration of $-SO_3^-$ in tethered MES [10]) appeared, but the peak at 2560 cm^{-1} (S–H stretching vibration of MES [18]) was not observed, confirming that the MES has been tethered to the TH units in ERGO–TH.

The above findings have been supported by SWASV experiments at the Bi/GCE, Bi/Nafion/GCE, Bi/Nafion/ERGO/GCE, Bi/Nafion/ERGO–TH/GCE, and Bi/Nafion/ERGO–TH–MES/GCE in 0.10 M acetate buffer (pH 4.5) containing 20.0 g L^{-1} Cd^{2+} and Pb^{2+}, and 400 g L^{-1} Bi^{3+}, as shown in Fig. 5. Both heights of the stripping peaks of Cd^{2+} and Pb^{2+} obeyed the order of Bi/GCE < Bi/Nafion/GCE < Bi/Nafion/ERGO/GCE < Bi/Nafion/ERGO–TH/GCE < Bi/Nafion/ERGO–TH–MES/GCE. Since the Bi/Nafion/ERGO–TH–MES/GCE exhibited the highest sensitivity and the best stability for assay of Cd^{2+} and Pb^{2+}, thus it was adopted in the following experiments.

At Nafion/ERGO–TH–MES/GCE or Nafion/ERGO–TH–MES/QCM Au electrode, the sulfonic group of MES can electrostatically attract Cd^{2+} and Pb^{2+} cations (electrostatic factor), the sulfur atom can coordinate with Cd^{2+} and Pb^{2+} ions (coordination factor), and it is interesting to make clear which factor predominates the MES-enhanced sensitivity. After QCM quantification of the Nafion layer and the MES-tethered ERGO–TH according to the Sauerbrey equation [31], we obtained the molar ratio of sulfonic groups in Nafion to those in MES-tethered ERGO–TH to be 2.8:1, thus the electrostatic factor of the sulfonic groups in MES-tethered ERGO–TH that account only for 26.3% in quantity should be the secondary. The ERGO–TH films with several thiols (MES, TGA or ME) similarly tethered at identical amount exhibited well comparable

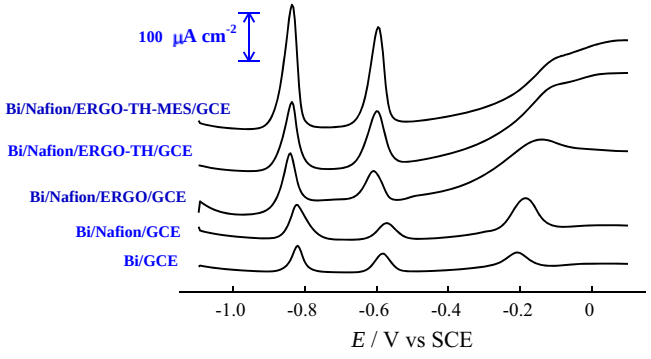

Fig. 5. Square wave anodic stripping voltammetry at bare GCE, Nafion/GCE, Nafion/ERGO/GCE, Nafion/ERGO–TH/GCE and Nafion/ERGO–TH–MES/GCE in 0.10 mol L^{-1} acetate buffer solution (pH 4.5) containing 20.0 μg L^{-1} each of Cd^{2+} and Pb^{2+}, and 400 μg L^{-1} bismuth. Deposition potential, −1.1 V; deposition time, 300 s; amplitude, 0.025 V; increment potential, 0.004 V; pulse period, 0.2 s.

stripping peaks (Fig. 6), suggesting that the coordination factor is predominant. Hence, the largest electrostatic effect of MES-tethered ERGO–TH in addition to the coordination effect results in its largest stripping peak here [10,29]. In addition, as shown in Fig. 5, the electrode modification of ERGO can notably enhance the anodic stripping heights (Bi/Nafion/ERGO/GCE versus Bi/Nafion/GCE), thus we also conclude that the high active surface area of ERGO contributes largely to the high analytical performance of our electrode. Hence, from Figs. 5 and 6, many factors contributed to the final performance of our electrode, and an individual modification of them cannot achieve a jump-like performance improvement of the modified electrode.

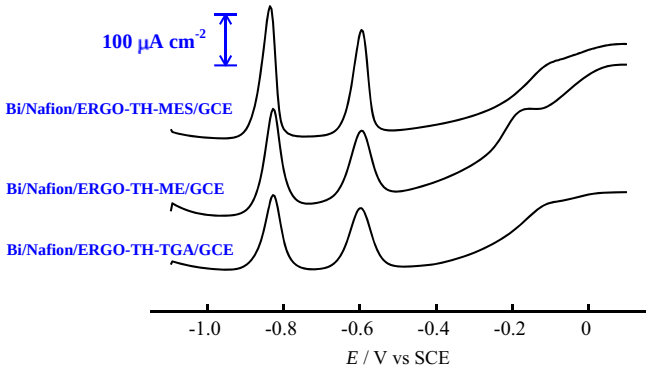

Fig. 6. Square wave anodic stripping voltammetry at Nafion/ERGO–TH–MES/GCE, Nafion/ERGO–TH–ME/GCE and Nafion/ERGO–TH–TGA/GCE, in 0.10 mol L^{-1} acetate buffer solution (pH 4.5) containing 20.0 μg L^{-1} each of Cd^{2+} and Pb^{2+}, and 400 μg L^{-1} bismuth. Other experimental conditions are the same as in Fig. 5.

3.2. SWASV determination of Cd^{2+} and Pb^{2+}

The pH of the background solution, the concentration of Bi^{3+}, the preconcentration potential, and the preconcentration time were optimized. The pH effect of the acetate buffer solution from 3.5 to 5.5 was investigated, as shown in Fig. S4A. The ASV peak current showed a peak-type response with maximum value at pH 4.5. The exact reason for this observation is not very clear at present, but the tendency can be understood as follows. A too low pH value should not be beneficial for ionization of the carboxyl groups of MES to electrostatically enrich cationic Cd^{2+} and Pb^{2+} ions and for a minimized hydrogen-evolution effect at the cathodic preconcentration potential of −1.1 V, and a too high pH value can result in hydrolysis of Cd^{2+} and Pb^{2+} ions and/or more swelling of the anionic Nafion/ERGO–TH–MES film. The optimal pH for analysis of Cd^{2+} and Pb^{2+} ions was thus selected to be pH 4.5. The influence of Bi^{3+} concentration on the peak current of Cd^{2+} and Pb^{2+} was studied in the range 200–600 μg L^{-1} and the optimal concentration of coexisting Bi^{3+} was 400 μg L^{-1}, as shown in Fig. S4B. The effect of concentration of coexisting Bi^{3+} is explained as follows. A too low Bi^{3+} concentration is not beneficial for the efficient formation of Bi alloys with atomic Pb and Cd to decrease the activation energy for cathodic preconcentration of atomic Pb and Cd, a too high Bi^{3+} concentration can lead to more obvious

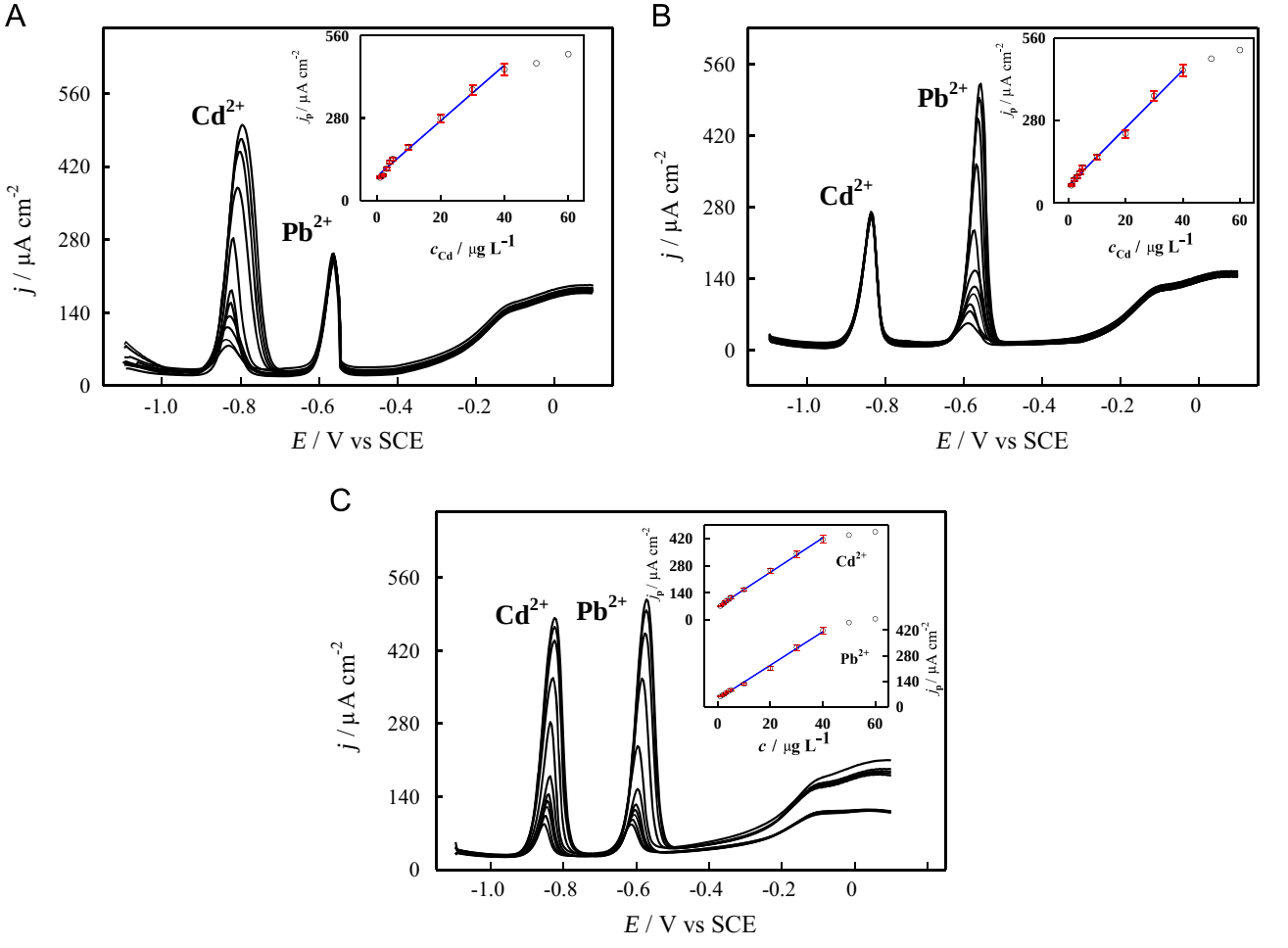

Fig. 7. Square wave anodic stripping voltammetric and calibration curves (Insets) on Bi/Nafion/ERGO–TH–MES/GCE for Cd^{2+} (A), Pb^{2+} (B), and both (C) at different concentrations in acetate buffer (pH 4.5) containing 300 μg L^{-1} Bi^{3+}. Other experimental conditions are the same as in Fig. 5.

Table 1
Limits of detection of Cd^{2+} and Pb^{2+} by anodic stripping voltammetry at Bi film modified electrodes.

Electrode	Analytical technique	Limit of detection ($\mu g\ L^{-1}$)		Reference
		Cd^{2+}	Pb^{2+}	
Bi/ABTS-MWCNTs/GCE	DPV	0.2	0.1	[2]
Bi/Nafion/GCE	SWV	0.1	0.1	[32]
Bi/GCE	SWV	0.2	0.2	[33]
Bi-plated carbon paste mini-electrodes	DPV	0.15	0.16	[34]
Bi/Nafion/2,2-bipyridyl/GCE	SWV	0.12	0.077	[35]
Bi/poly(*p*-aminobenzene sulfonic acid) film electrode	DPV	0.63	0.80	[36]
Lithographically fabricated disposable bismuth-film electrode	SWV	1.0	0.50	[37]
bismuth-modified zeolite doped carbon paste electrode	DPV	0.08	0.10	[38]
Bi/Nafion/ERGO–TH–MES/GCE	SWV	0.1	0.05	This work

*ABTS: 2,2'-azinobis (3-ethylbenzothiazoline-6-sulfonate).

Table 2
Determination of Cd^{2+} and Pb^{2+} in real samples ($n=5$).

Sample	Original Cd^{2+} ($\mu g\ L^{-1}$)	Original Pb^{2+} ($\mu g\ L^{-1}$)	Added Cd^{2+} ($\mu g\ L^{-1}$)	Added Pb^{2+} ($\mu g\ L^{-1}$)	Cd^{2+}			Pb^{2+}		
					Found ($\mu g\ L^{-1}$)	Recovery (%)	RSD (%)	Found ($\mu g\ L^{-1}$)	Recovery (%)	RSD (%)
a	–	2.70	10.00	10.00	9.43	94.3	4.1	11.2	112	5.0
b	–	1.15	10.00	10.00	10.7	107	3.8	9.57	95.7	3.4
c	–	0.64	10.00	10.00	10.8	108	3.7	10.3	103	3.1

a, Xiangjiang river water; b, Yuelu spring water; c, tap water.

competitive binding of Bi^{3+} at the active adsorption sites of the film against binding of Pb^{2+} and Cd^{2+} to achieve an enhanced ASV-analysis sensitivity, and thus a peak-type response to Bi^{3+} concentration was observed. The effect of preconcentration potential on the stripping peak current of Cd^{2+} and Pb^{2+} was studied in the range from -1.0 to -1.4 V, as shown in Fig. S4C, and an optimal preconcentration potential of -1.1 V is recommended for the following study. Here, a preconcentration potential as negative as possible can maximize the preconcentration efficiency of Cd^{2+} and Pb^{2+} ions but a too negative preconcentration potential should increase the interfering hydrogen-evolution effect, thus a peak-type response of the preconcentration potential was observed. Moreover, the effect of the preconcentration time was examined. The stripping responses increased almost linearly with the increase of preconcentration time firstly, and after 300 s the ASV signal increased a little, indicating a notably decreased preconcentration efficiency after 300 s due probably to the exhaustion of solution-state Cd^{2+} and Pb^{2+} analytes, as shown in Fig. S4D. Taking both the sensitivity and the time cost into account, the preconcentration time for 300 s was chosen in the experiments. Considering the preconcentration time, the equilibration period, the time for the SWASV sweep, and the subsequent electrochemical rinse of the electrode, it generally took ca. 400 s to finish one run of SWASV experiment.

Under the optimal conditions (Fig. S4), simultaneous analysis of Cd^{2+} and Pb^{2+} was performed, as shown in Fig. 7. First, analysis of Cd^{2+} and Pb^{2+} was performed by changing the concentration of one species, whereas remaining that of the other species constant. As shown in Fig. 7A, the peak current of Cd^{2+} is linear with its concentration from 1 to 40 $\mu g\ L^{-1}$ at a sensitivity (slope) of 9.48 $\mu A\ L\ \mu g^{-1}\ cm^{-2}$ (versus geometric area of the disk GCE) when the concentrations of Pb^{2+} and Bi^{3+} were fixed at 20.0 $\mu g\ L^{-1}$ and 400 $\mu g\ L^{-1}$, respectively. The responses of Pb^{2+} are practically unaltered with the increase of Cd^{2+} concentration. Similarly, keeping the concentrations of Cd^{2+} constant, the peak current of Pb^{2+} is linear with its concentration in the range of 1–40 $\mu g\ L^{-1}$ at a sensitivity of 9.90 $\mu A\ L\ \mu g^{-1}\ cm^{-2}$, as shown in Fig. 7B. Limits of detection ($S/N=3$) of 0.1 $\mu g\ L^{-1}$ for Cd^{2+} and 0.05 $\mu g\ L^{-1}$ Pb^{2+} were obtained after 5-min preconcentration. Second, analysis of Cd^{2+} and Pb^{2+} was performed at varying concentrations for both, as shown in Fig. 7C. The peak currents increased linearly with the metal concentration with a slope of 9.05 $\mu A\ L\ \mu g^{-1}\ cm^{-2}$ for Cd^{2+} and 9.34 $\mu A\ L\ \mu g^{-1}\ cm^{-2}$ for Pb^{2+}. The sensitivities in the above determinations for either Cd^{2+} or Pb^{2+} were comparable with each other, implying that simultaneous analysis of Cd^{2+} and Pb^{2+} is feasible. Limits of detection of Cd^{2+} and Pb^{2+} in our work are amongst the lowest ones reported previously (Table 1). The relative standard deviations (RSDs) for five successive determinations of 20.0 $\mu g\ L^{-1}$ Cd^{2+} and 20.0 $\mu g\ L^{-1}$ Pb^{2+} were 4.4% for Cd^{2+} and 5.3% for Pb^{2+} under optimized conditions. We also found that 1000-fold mass ratio of K^+, Na^+, Ca^{2+}, Mg^{2+}, Cl^-, and SO_4^{2-}, and 30-fold mass ratio of Co^{2+}, Ni^{2+}, Zn^{2+}, Ag^+, Cu^{2+}, and Hg^{2+} caused no obvious signal changes for 20.0 $\mu g\ L^{-1}$ Cd^{2+} and 20.0 $\mu g\ L^{-1}$ Pb^{2+} under optimized conditions.

To illustrate the application potential of Bi/Nafion/ERGO–TH–MES/GCE in practical analysis, the electrode was employed for the simultaneous determination of Cd^{2+} and Pb^{2+} in three real samples from local environment, tap water, spring water from Yuelu mountain, and water from Xiangjiang river. All water samples were filtered with a 0.22 μm membrane (purchased from Millipore) in advance, and then added to 0.10 M acetate buffer (pH 4.5) containing 400 $\mu g\ L^{-1}$ Bi^{3+} (2.5-fold dilution). The anodic stripping peak currents were recorded for the determination of Cd^{2+} and Pb^{2+}, before and after the additions of their standard solutions to the samples under the same conditions. The results are illustrated in Table 2. In addition, our electrode has been validated with commercially available national standard aqueous samples of Cd^{2+} and Pb^{2+}, and we obtained within 6% deviations from the reference results (diluted to 20.0 $\mu g\ L^{-1}$ Pb^{2+} or Cd^{2+} for SWASV tests). The above results should imply that the Bi/Nafion/ERGO–TH–MES/GCE has great potential application in real water samples.

4. Conclusions

In summary, we have prepared a new ERGO–TH–MES nanocomposite via thiolation. A GCE modified with ERGO–TH–MES, Nafion and Bi has been developed to simultaneously and sensitively determine Cd^{2+} and Pb^{2+} using the SWASV method. The reaction between ERGO–TH and MES has been investigated by the EQCM and spectroscopic methods. We believe that the functional nanocomposites based on the thiol–ene chemistry may offer high application potential to treatment and analysis of environmental heavy metals.

Acknowledgments

This work was supported by the National Natural Science Foundation of China (21175042, 21075036), Hunan Lotus Scholars Program, the Foundations of Hunan Provincial Education and Science/Technology Department, Program for Science and Technology Innovative Research Team in Higher Educational Institutions of Hunan Province and Key Laboratory of Jiangxi Province for Persistent Pollutants Control and Resources Recycling. Z. Li and L. Chen contributed equally to this work.

Appendix A. Supporting information

Supplementary data associated with this article can be found in the online version at http://dx.doi.org/10.1016/j.talanta.2014.01.062.

References

[1] J. Li, S. Guo, Y. Zhai, E. Wang, Anal. Chim. Acta 649 (2009) 196–201.
[2] W. Deng, Y. Tan, Z. Fang, Q. Xie, Y. Li, X. Liang, S. Yao, Electroanalysis 21 (2009) 2477–2485.
[3] H. Xu, L. Zeng, S. Xing, Y. Xian, G. Shi, L. Jin, Electroanalysis 20 (2008) 2655–2662.
[4] L. Jiang, Y. Wang, J. Ding, T. Lou, W. Qin, Electrochem. Commun. 12 (2010) 202–205.
[5] J. Wang, J. Lu, S.B. Hocevar, P.A.M. Farias, B. Ogorevc, Anal. Chem. 72 (2000) 3218–3222.
[6] J. Wang, Electroanalysis 17 (2005) 1341–1346.
[7] G.H. Hwang, W.K. Han, S.J. Hong, J.S. Park, S.G. Kang, Talanta 77 (2009) 1432–1436.
[8] G. Aragay, J. Pons, A. Merkoci, Chem. Rev. 111 (2011) 3433–3458.
[9] H. Zejli, J.L. Cisneros, I. Naranjo-Rodriguez, K.R. Temsamani, Talanta 71 (2007) 1594–1598.
[10] L. Chen, Z. Su, X. He, Y. Liu, C. Qin, Y. Zhou, Z. Li, L. Wang, Q. Xie, S. Yao, Electrochem. Commun. 15 (2012) 34–37.
[11] Z.M. Wang, H.W. Guo, E. Liu, G.C. Yang, N.W. Khun, Electroanalysis 22 (2009) 209–215.
[12] K. Novoselov, A. Geim, S. Morozov, D. Jiang, Y. Zhang, S. Dubonos, I. Grigorieva, A. Firsov, Science 306 (2004) 666–669.
[13] C. Chen, W. Zhai, D. Lu, H. Zhang, W. Zheng, Mater. Res. Bull. 46 (2011) 583–587.
[14] Q. Wei, K. Mao, D. Wu, Y. Dai, J. Yang, B. Du, M. Yang, H. Li, Sens. Actuator B: Chem. 149 (2010) 314–318.
[15] F.Y. Kong, X.R. Li, W.W. Zhao, J.J. Xu, H.Y. Chen, Electrochem. Commun. 14 (2012) 59–62.
[16] C.E. Hoyle, A.B. Lowe, C.N. Bowman, Chem. Soc. Rev. 39 (2010) 1355–1387.
[17] C.E. Hoyle, C.N. Bowman, Angew. Chem. Int. Ed. 49 (2010) 1540–1573.
[18] Z. Su, J. Huang, Q. Xie, Z. Fang, C. Zhou, Q. Zhou, S. Yao, Phys. Chem. Chem. Phys. 11 (2009) 9050–9061.
[19] Q. Xie, J. Wang, A. Zhou, Y. Zhang, H. Liu, Z. Xu, Y. Yuan, M. Deng, S. Yao, Anal. Chem. 71 (1999) 4649–4656.
[20] O. Zaouak, L. Authier, C. Cugnet, A. Castetbon, M. Potin-Gautier, Electroanalysis 21 (2009) 689–695.
[21] D.A. Buttry, M.D. Ward, Chem. Rev. 92 (1992) 1355–1379.
[22] X. Tu, Q. Xie, C. Xiang, Y. Zhang, S. Yao, J. Phys. Chem. B 109 (2005) 4053–4063.
[23] Q. Xie, C. Xiang, Y. Yuan, Y. Zhang, L. Nie, S. Yao, J. Colloid Interface Sci. 262 (2003) 107–115.
[24] C. Deng, M. Li, Q. Xie, M. Liu, Y. Tan, X. Xu, S. Yao, Anal. Chim. Acta 557 (2006) 85–94.
[25] X. He, Z. Su, Q. Xie, C. Chen, Y. Fu, L. Chen, Y. Liu, M. Ma, L. Deng, D. Qin, Microchim. Acta 173 (2011) 95–102.
[26] A.A. Karyakin, E.E. Karyakina, H.L. Schmidt, Electroanalysis 11 (1999) 149–155.
[27] Z. Sun, H. Fu, L. Deng, J. Wang, Anal. Chim. Acta 761 (2013) 84–91.
[28] F.Y. Kong, M.T. Xu, J.J. Xu, H.Y. Chen, Talanta 85 (2011) 2620–2625.
[29] G. Herzog, D.W. Arrigan, Anal. Chem. 75 (2003) 319–323.
[30] Z. Li, Y. Huang, L. Chen, X. Qin, Z. Huang, Y. Zhou, Y. Meng, J. Li, S. Huang, Y. Liu, W. Wang, Q. Xie, S. Yao, Sens. Actuator B: Chem. 181 (2013) 280–287.
[31] Q. Xie, Z. Li, C. Deng, M. Liu, Y. Zhang, M. Ma, S. Xia, X. Xiao, D. Yin, S. Yao, J. Chem. Educ. 84 (2007) 681–684.
[32] G. Kefala, A. Economou, A. Voulgaropoulos, Analyst 129 (2004) 1082–1090.
[33] G.H. Hwang, W.K. Han, S.J. Hong, J.S. Park, S.G. Kang, Talanta 77 (2009) 1432–1436.
[34] L. Baldrianova, I. Svancara, S. Sotiropoulos, Anal. Chim. Acta 599 (2007) 249–255.
[35] F. Torma, M. Kádár, K. Tóth, E. Tatár, Anal. Chim. Acta 619 (2008) 173–182.
[36] Y. Wu, N.B. Li, H.Q. Luo, Sens. Actuator B: Chem. 133 (2008) 677–681.
[37] C. Kokkinos, A. Economou, I. Raptis, C.E. Efstathiou, Electrochim. Acta 53 (2008) 5294–5299.
[38] L. Cao, J. Jia, Z. Wang, Electrochim. Acta 53 (2008) 2177–2182.